PRODUCING EXCITED ELECTRONIC LEVELS IN OXYGEN BY THE BEAM-FOIL METHOD

NSG-628

by

Kenneth Shrum Burton

A Thesis Submitted to the Faculty of the

DEPARTMENT OF PHYSICS

In Partial Fulfillment of the Requirements
For the Degree of

MASTER OF SCIENCE

In the Graduate College

THE UNIVERSITY OF ARIZONA

1967

STATEMENT BY AUTHOR

This thesis has been submitted in partial fulfillment of requirements for an advanced degree at The University of Arizona and is deposited in the University Library to be made available to borrowers under rules of the Library.

Brief quotations from this thesis are allowable without special permission, provided that accurate acknowledgment of the source is made. Requests for permission for extended quotation from or reproduction of this manuscript in whole or in part may be granted by the head of the major department or the Dean of the Graduate College when in his judgment the proposed use of the material is in the interests of scholarship. In all other instances, however, permission must be obtained from the author.

SIGNED: _____

APPROVAL BY THESIS DIRECTOR

This thesis has been approved on the date shown below:

_____ _____

S. BASHKIN DATE

Professor of Physics

ACKNOWLEDGMENTS

The author wishes to express his gratitude to Professor Stanley Bashkin for his valuable guidance in the work undertaken, to Professor William Bickel and Mr. Keith Masterson for their assistance in conducting the experimental work. He also wishes to thank Steward Observatory for the use of the Hilger-Watts Densitometer, Kitt Peak Observatory for the use of the Meinel Spectrograph and the Grant Comparator, and the National Aeronautics and Space Administration for its financial support.

TABLE OF CONTENTS

LIST OF TABLES

LIST OF ILLUSTRATIONS

ABSTRACT

The thin foil ionic beam technique was used to produce a beam of multiply ionized and excited oxygen ions. Excited levels produced by collisions in the foil were detected by wavelength measurements of the emitted spectral lines as recorded on photographic plates. Excitation functions of various levels were obtained from the spectral lines using microdensitometer techniques. It was found that populations agreed within experimental error with theoretical line strengths. However, the populations of the excited levels do not obey a Boltzmann distribution. Excitation functions were found to reach peaks at particle energies of about 0.50 MeV in O II and 0.63 MeV in O III.

I. INTRODUCTION

The main sources of excited particles previously used for spectroscopic investigations of atomic properties have been flames, arcs, sparks, discharge tubes and plasmas. Bashkin[1] proposed that thin foils used as targets for ionic beams could be used as a spectroscopic source. The thin foil technique has the following advantages:

1. The spectra which result from photon emission in the decay of the excited levels are time-resolved.
2. The only mode of decay is spontaneous emission of a photon since the particle density in the beam and the ambient vacuum are sufficiently low to insure no interaction between particles. Further, recombination lines are not observed because the electron density in the beam is low.
3. Since an accelerated ionic beam is the spectroscopic source, the common techniques of electrostatic or magnetic analysis of the beam insure a chemically pure source.
4. Ionizations and excitations of beam particles by the foil depend on the energy of the incident particles, and it is possible to obtain high ionizations by using beam energies of a few MeV.
5. Essentially all the chemical elements can be studied under identical excitation conditions.

The excitation function of an excited level is defined as the relative initial population of the excited level as a function of energy of the incoming particles. For thermal sources such as flames, arcs, sparks and plasmas, level populations are proportional to exp $(- E_n/kT)$, where E_n is the energy of the n'th excited level, k is Boltzmann's constant, and T is the absolute temperature of the source.[2] Although it is not possible to assign a temperature to the beam particles, it is of interest to compare the level populations as functions of beam energy for foil-excited particles with the level populations as functions of temperature for other techniques.

II. EXPERIMENT

A beam of singly-ionized, diatomic oxygen molecules was accelerated to the desired energy using a 2 MV Van de Graaff accelerator. The beam was passed through an analyzing magnet which directed the particles with the proper p/e ratio into the target chamber and through a thin carbon foil. In the above, p is the momentum of the particles and e is the net electronic charge. Collisions in the foil reduced the oxygen molecular ion beam to a monatomic beam, and the oxygen particles emerged from the foil with some distribution of ionization and excitation. The excited particles decayed by spontaneous emission of a photon; the photons were dispersed with the f/0.8 stigmatic Meinel spectrograph and were recorded on photographic plates. Kodak 103a-o spectroscopic plates were used. Exposure times ranged from 5 minutes to 90 minutes with beam currents of about 0.3 μamps. Due to the use of glass lenses in the optical system and to the sensitivities of the photographic plates, the wavelength region examined was from 3600 Å to 4700 Å. The experimental arrangement is shown in Fig. 1.

Since the Meinel spectrograph is a stigmatic instrument, each spectral line appears as an image of the slit of the spectrograph, with each point of the line corresponding to a point in the beam. The lines will be darkest at the foil end and will decrease in intensity along their length due to the exponential decay of the ions and to the stigmatic property of the spectrograph. Thus

measurement of the density of a spectral line at some distance from the foil end of the line corresponds to a measurement of the number of photons emitted at some distance downstream from the foil.

The relative populations of the various levels were obtained from the photographic plates by determining the relative powers of the spectral lines. Since density rather than emitted power must be measured from the spectral lines, it was necessary to relate density to power using black-body continuum plates. A tungsten filament lamp operated at 1950°K ± 50°K was used as the black-body source, and a step-density filter was used to obtain various densities. The exposure times of the black-body plates were the same as the exposure times of the corresponding spectral plates. Figure 2 shows a spectral plate taken with an O_2^+ beam at 1.0 MeV and the corresponding black-body plate.

To compare spectral plates taken with different beam currents and beam energies, it was necessary to determine the number of particles passing through the foil for each exposure. This was done by integrating the beam current collected by a shielded Faraday cup, and recording the total charge for the plate. The total charge could then be converted to the total number of particles passing through the foil by using measurements of relative charge state populations in the beam as a function of beam energy.[3]

To aid in wavelength determination, an iron-argon comparison spectrum was taken on each spectral plate and on each black-body plate as shown in Fig. 2. The wavelengths of the spectral

lines were measured to an accuracy of ± 0.5 Å using a Grant Comparator, and the transitions giving the spectral lines were then determined using tables of previously observed transitions[4] and wavelengths computed from energy level tables.[5] In Tables 1, 2, and 3, the observed spectral lines are numbered and wavelengths and transitions of the lines are listed.

III. ANALYSIS

Since the spectral lines are time resolved, it is possible to determine populations of the levels soon after the ions are excited in the foil by measuring relative power at the foil end of the spectral lines. Measurements of the densities of the spectral lines were made with a Hilger-Watts densitometer. The slit width of the densitometer corresponded to a distance along the beam of 1.2 mm and the measurements were made with the center of the slit at a position on the line which corresponded to a beam distance of 1.0 mm from the foil. A typical densitometer scan is shown in Fig. 3. For the following reason, no correction was made for the error due to decay of the beam in this distance. Study of the spectral lines shows that on several lines the change in emitted power does not follow an exponential decay until the beam particles are as far as 1.5 mm from the foil. Cascading from higher levels is known to be present in many cases and is probably the source of the difficulty. Much more extensive measurements would be necessary to correct for this problem.

The expression used to determine relative populations from the measured densities of the spectral lines is derived below. Consider a spectral plate taken at a beam energy E and exposed for a time t with integrated beam charge Q. A given level with initial population N can in general decay to several lower levels with

each decay being characterized by its wavelength λ and spontaneous emission coefficient A. These various decays can frequently be resolved on the spectral plates, and the population of the upper level can be determined from the examination of a single spectral line. In such a case, the population N is given by

$$N = \frac{\lambda P}{hcA} \quad , \tag{1}$$

where P is the power of the line, λ is the wavelength of the line, h is Planck's constant, c is the speed of light, and A is the spontaneous emission coefficient for the transition.

In Eq. (1), all quantities are constant for a given transition except the power P. As indicated previously, density of the spectral line must be directly measured rather than power, and the emitted power is then obtained using the black-body continuum plates. This was done as follows: the power of the line is related to the density by

$$P = \frac{\rho \, H(\lambda, t, \text{geom})}{t} \tag{2}$$

where ρ is the density of the line at the foil, t is the exposure time, and $H(\lambda, t, \text{geom})$ is a function which includes corrections for the geometry of the system and for plate exposure characteristics. On the black-body plates, the step-density filter caused the plate to be exposed in strips of different density, where each strip covered the entire wavelength region of the plate. The power emitted by the black-body is related to the plate density of a

given strip at a given wavelength by

$$P_o(\lambda) \quad \frac{\rho_o(\lambda)\ H(\lambda,\ t,\ \text{geom})}{\epsilon_o(\lambda)\ t} \tag{3}$$

where $P_o(\lambda)$ is the power of the black-body at wavelength λ, $\epsilon_o(\lambda)$ is the transmission of the corresponding step of the filter, $\rho_o(\lambda)$ is the density of the strip at λ, and H is the same function as in Eq. (2). From the densities $\rho_o(\lambda)$ for different strips, there will be an interpolated value of the transmission such that the density of the black-body continuum is equal to the density of the spectral line. This value of the transmission will be denoted by ϵ. Then from Eqs. (2) and (3) one obtains

$$P = P_o(\lambda)\ \epsilon \tag{4}$$

Substituting for P in Eq. (1) gives the relative population

$$N = \frac{P_o(\lambda)\ \epsilon\ \lambda}{hc\ A} \tag{5}$$

Since the average number of particles passing through the foil varied from plate to plate, it was necessary to normalize the initial populations to the number of particles passing through the foil, and to the velocities of the particles. In this experiment the number of particles passing through the foil was determined indirectly by measuring the number of charges collected by the Faraday cup. Let n be the number of particles which pass through the foil for one exposure. Let l indicate the charge states of the

ions, so $\ell = 0$ represents neutral particles, $\ell = 1$ represents singly ionized particles, etc. For a given energy E, a certain fraction F_ℓ of the beam particles will be in charge state ℓ, and the number of particles passing through the foil and being ionized into charge state ℓ will be nF_ℓ. The net charge collected will be

$$Q = \sum_\ell \ell(nF_\ell) \ . \tag{6}$$

Thus,

$$n = \frac{Q}{\sum_\ell \ell \, F_\ell} \tag{7}$$

It should be mentioned that the method used above for determining the number of particles is not the most convenient method. A more straightforward method would be to measure the integrated charge with the foil out of the beam, and with the foil in the beam. Since the integrated charge Q with the foil out is related to the number of particles by

$$Q = ne \ , \tag{8}$$

and since the ratio of integrated charge with foil out to charge with foil in is a constant for a given foil and given energy, the average number of particles passing through the foil per second is easily determined from the total integrated current with the foil in the beam.

The effect of different beam velocities can be seen from the following. Assume N particles are initially excited into a given level. Let the line be examined over an interval dx, where dx is less than one tenth of a mean decay distance. If the velocity of the beam is v_1, the number of atoms or ions observed to decay at the foil by a given transition is

$$dN_1 = N A \frac{dx}{v_1} \tag{9}$$

Now consider a beam of velocity v_2 but assume the particle flux through the foil is such that there are still initially N particles excited into a given level. Then the number of decays observed will be

$$dN_2 = N A \frac{dx}{v_2} \tag{10}$$

Thus,

$$v_1 \, dN_1 = v_2 \, dN_2 \tag{11}$$

Including the normalizations for the number of particles in the beam, and for the velocity of the particles, one obtains for the normalized power,

$$P' = P \frac{v}{n} = P_0(\lambda) \frac{\epsilon \, v \, \Sigma \, \ell \, F_\ell}{Q} , \tag{12}$$

and for the normalized relative populations

$$N' = N\frac{v}{n} = I_o(\lambda)\ \frac{\epsilon\ \lambda\ v\ \Sigma\ \ell\ F_\ell}{Hc\ A\ Q} \qquad (13)$$

Table 4 gives the values obtained from Eq. (12) for the normalized powers, and Table 5 gives the values of the relative populations calculated from Eq. (13). The values of the emission coefficients were obtained from tables of experimentally-determined transition probabilities.[6]

In order to determine the errors in the measured values of the emitted powers, two separate exposures made with the same beam energy were compared. From this comparison, it was found that the errors are less than 25%. In calculating relative populations, the transition probabilities used were given as being correct to within 25%. Thus, the populations should be correct to within 43%.

IV. RESULTS

From Tables 1, 2 and 3, one finds that 80 lines were observed in the wavelength region 3600 Å to 4700 Å. The majority of these transitions were observed in O II, with only three multiplets observed in O III, and one multiplet observed in O IV. There were no transitions observed which could be definitely identified as coming from O I or O V. This was unexpected for O I since the charge state population of O I at low energies is over 15% of the total beam.[3]

From the data it does not appear that foil excited particles obey a Boltzmann distribution. This can be seen from "non-degenerate" state populations obtained by dividing the level populations by $(2S + 1)(2J + 1)$. If the foil excited particles had a distribution similar to a Boltzmann distribution, one would see an exponential decrease in populations in a charge state, and between charge states. This definitely is not observed from these data. In Table 6, the "non-degenerate" state populations are given for oxygen particles at 0.50 MeV.

From Tables 1 through 4 it is seen that in almost all multiplets, the most powerful lines observed are those corresponding to the higher J transitions with $\Delta J = \Delta L$. This agrees qualitatively with theoretical calculations of line strengths, assuming LS coupling. Line strengths rather than powers are generally calculated theoretically since line strength is the more fundamental

quantity. The line strength for a transition from level a to level b is defined as

$$S(a, b) = \sum_{\alpha,\beta} [(\alpha \, |\vec{P}| \, \beta)]^2 , \qquad (14)$$

where $(\alpha \, |\vec{P}| \, \beta)$ is the matrix element for a dipole transition from level a with quantum numbers α to level b with quantum numbers β.[7] The emitted power P is related to the line strength S(a, b) by

$$P = \frac{N(a)\, 64\, \pi^4 c}{(2J + 1)\, \lambda^4} \, S(a, b) . \qquad (15)$$

It is of interest to compare powers of lines originating on the same level, and to compare populations of the level as calculated from these powers. There are four pairs of lines observed where each pair originates on a single level, and in Table 7 the ratios of the powers of these lines are compared with ratios of line strengths. This comparison is independent of the population and thus does not include the errors introduced by the transition probabilities. From this table one sees that the powers do agree with the ratios of line strengths within experimental error. From Table 5, the agreement between populations calculated from the pairs of lines is not found to be as good, although in two of the cases, they do agree within experimental error.

The dependence of the populations of the levels on energy can be seen from Table 3. In particular, the populations of the levels in O II increase with energy from 0.20 MeV per particle to

about 0.50 MeV per particle and then decrease, with about a factor of 2 change in population. For O III, the peak populations occur at about 0.63 MeV per particle, where they are about three times the populations at 0.20 MeV. In Figs. 4 through 7, populations obtained from lines 3, 15, 29 and 43 are shown as a function of beam energy.

V. CONCLUSION

Using the thin foil technique for producing excited levels, it is found that the different J levels in a multiplet are populated as expected from the calculated line strengths, and that ratios of powers agree within experimental error with ratios of line strengths for transitions from a single level. However, the populations of the levels do not follow a Boltzmann distribution.

Populations of the levels show a dependence on beam energy with the populations in O II and O III reaching a maximum at about 0.50 MeV and 0.63 MeV per particle respectively. The maximum variations in populations in the energy range investigated are about a factor of two for O II lines and a factor of three for O III lines.

Table 1. Wavelengths and Transitions of Lines Observed in Ionization State O II.

Line No.	Measured Wavelength (Å)	Identified Wavelength (Å)	Multiplet	Transition Final	Transition Initial	$J_f - J_i$
79	4650.4	4650.34	1	$3s\ ^4P$	$3p\ ^4D^o$	5/2 - 7/2
78	4643.1	4643.01	1	$3s\ ^4P$	$3p\ ^4D^o$	3/2 - 5/2
77	4670.3	4670.05	1	$3s\ ^4P$	$3p\ ^4D^o$	1/2 - 3/2
80	4662.5	4662.84	1	$3s\ ^4P$	$3p\ ^4D^o$	3/2 - 3/2
51	4351.0	4350.66	2	$3s\ ^4P$	$3p\ ^4P^o$	5/2 - 5/2
54	4368.4	4368.13	2	$3s\ ^4P$	$3p\ ^4P^o$	5/2 - 3/2
50	4366.2	4346.65	2	$3s\ ^4P$	$3p\ ^4P^o$	3/2 - 1/2
12	3750.5	3750.55	3	$3s\ ^4P$	$3p\ ^4S^o$	5/2 - 3/2
9	3728.1	3728.39	3	$3s\ ^4P$	$3p\ ^4S^o$	3/2 - 3/2
5	3713.7	3713.77	3	$3s\ ^4P$	$3p\ ^4S^o$	1/2 - 3/2
62	4416.2	4416.12	5	$3s\ ^2P$	$3p\ ^2D^o$	3/2 - 5/2
63	4418.5	4418.20	5	$3s\ ^2P$	$3p\ ^2D^o$	5/2 - 7/2
69	4453.3	4453.71	5	$3s\ ^2P$	$3p\ ^2D^o$	3/2 - 3/2
29	3974.4	3974.39	6	$3s\ ^2P$	$3p\ ^2P^o$	3/2 - 3/2
27	3955.0	3955.48	6	$3s\ ^2P$	$3p\ ^2P^o$	1/2 - 1/2
25	3946.0	3946.16	6	$3s\ ^2P$	$3p\ ^2P^o$	1/2 - 3/2
34	4077.0	4077.02	10	$3p\ ^4D^o$	$3d\ ^4F$	7/2 - 9/2
33	4073.3	4073.30	10	$3p\ ^4D^o$	$3d\ ^4F$	5/2 - 7/2
32	4071.1	4071.04	10	$3p\ ^4D^o$	$3d\ ^4F$	3/2 - 5/2
32	4071.1	4070.79	10	$3p\ ^4D^o$	$3d\ ^4F$	1/2 - 3/2
36	4085.1	4086.27	10	$3p\ ^4D^o$	$3d\ ^4F$	5/2 - 5/2

Table 1--Continued

Line No.	Measured Wavelength (Å)	Identified Wavelength (Å)	Multiplet	Transition Final	Transition Initial	$J_f - J_i$
35	4079.7	4080.02	10	$3p\ ^4D^o$	$3d\ ^4F$	3/2 - 3/2
22	3908.2	3908.55	11	$3p\ ^4D^o$	$3d\ ^4P$	5/2 - 5/2
21	3883.6	3883.54	11	$3p\ ^4D^o$	$3d\ ^4P$	3/2 - 3/2
21	3883.6	3883.29	12	$3p\ ^4D^o$	$3d\ ^4D$	7/2 - 7/2
20	3849.5	3848.98	12	$3p\ ^4D^o$	$3d\ ^4D$	1/2 - 1/2
75	4592.1	4592.46	15	$3s'\ ^2D$	$3p^1\ ^2F^o$	5/2 - 7/2
76	4597.2	4597.28	15	$3s'\ ^2D$	$3p^1\ ^2F^o$	3/2 - 5/2
76	4597.2	4597.49	15	$3s'\ ^2D$	$3p^1\ ^2F^o$	5/2 - 5/2
52	4352.5	4352.50	16	$3s'\ ^2D$	$3p^1\ ^2D^o$	5/2 - 5/2
52	4352.5	4352.69	16	$3s'\ ^2D$	$3p^1\ ^2D^o$	3/2 - 5/2
23	3912.8	3913.07	17	$3s'\ ^2D$	$3p^1\ ^2P^o$	5/2 - 3/2
24	3920.1	3920.37	17	$3s'\ ^2D$	$3p^1\ ^2P^o$	3/2 - 1/2
23	3912.8	3913.22	17	$3s'\ ^2D$	$3p^1\ ^2P^o$	3/2 - 3/2
41	4155.3	4154.45	19	$3p\ ^4P^o$	$3d\ ^4P$	3/2 - 5/2
39	4120.5	4120.38	20	$3p\ ^4P^o$	$3d\ ^4D$	5/2 - 7/2
38	4098.1	4098.39	20	$3p\ ^4P^o$	$3d\ ^4D$	1/2 - 3/2
60	4397.4	4397.19	26	$3p\ ^2D^o$	$3d\ ^2D$	5/2 - 5/2
55	4370.5	4370.53	26	$3p\ ^2D^o$	$3d\ ^2D$	3/2 - 3/2
61	4409.6	4407.26	26	$3p\ ^2D^o$	$3d\ ^2D$	5/2 - 3/2
53	4361.5	4360.58	26	$3p\ ^2D^o$	$3d\ ^2D$	3/2 - 5/2
68	4449.2	4449.59	35	$3p'\ ^2F^o$	$3d^1\ ^2F$	7/2 - 7/2
43	4191.0	4190.97	36	$3p'\ ^2F^o$	$3d^1\ ^2G$	7/2 - 9/2

Table 1--Continued

Line No.	Measured Wavelength (Å)	Identified Wavelength (Å)	Multiplet	Transition Final — Initial	$J_f - J_i$
42	4186.6	4186.62	36	$3p'\ ^2F^o - 3d^1\ ^2G$	5/2 - 7/2
43	4191.0	4190.76	36	$3p'\ ^2F^o - 3d^1\ ^2G$	7/2 - 7/2
28	3963.6	3964.18	43	$3p'\ ^2D^o - 4d\ ^2P$	5/2 - 3/2
26	3949.6	3950.51	43	$3p'\ ^2D^o - 4d\ ^2P$	3/2 - 1/2
37	4090.4	4090.44	48	$3d\ ^4F - 4f\ ^4G^o$	9/2 - 11/2
38	4098.8	4098.43	48	$3d\ ^4F - 4f\ ^4G^o$	7/2 - 9/2
31	4066.0	4066.22	50	$3d\ ^4F - 4f\ ^4F^o$	9/2 - 7/2
47	4305.0	4305.04	54	$3d\ ^4P - 4f\ ^4D^o$	5/2 - 7/2
45	4278.0	4277.90	54	$3d\ ^4P - 4f\ ^4D^o$	3/2 - 1/2
73	4470.3	4470.50	59	$3p'\ ^2P^o - 4d\ ^4D$	3/2 - 5/2
48	4316.3	4316.48	64	$3d\ ^4D - 4f\ ^4D^o$	3/2 - 3/2
48	4316.3	4316.67	64	$3d\ ^4D - 4f\ ^4D^o$	3/2 - 1/2
48	4316.3	4316.77	64	$3d\ ^4D - 4f\ ^4D^o$	5/2 - 3/2
45	4278.0	4277.97	67	$3d\ ^4D - 4f\ ^4F^o$	5/2 - 7/2
46	4285.0	4284.16	67	$3d\ ^4D - 4f\ ^4F^o$	3/2 - 5/2
46	4285.0	4284.33	67	$3d\ ^4D - 4f\ ^4F^o$	5/2 - 5/2
46	4285.0	4284.95	67	$3d\ ^4D - 4f\ ^4F^o$	3/2 - 3/2
49	4342.4	4343.23	77	$3d\ ^2F - 4f\ ^2G^o$	7/2 - 9/2
48	4316.3	4316.57	79	$3d\ ^2F - 4f\ ^2F^o$	7/2 - 5/2
30	4061.9	4061.67	97	$3d'\ ^2F - 4f^1\ ^2G^o$	7/2 - 9/2
30	4061.9	4062.20	97	$3d'\ ^2F - 4f^1\ ^2G^o$	5/2 - 7/2
30	4061.9	4061.67	97	$3d'\ ^2F - 4f^1\ ^2G^o$	7/2 - 7/2

Table 1--Continued

Line No.	Measured Wavelength (Å)	Identified Wavelength (Å)	Multiplet	Transition Final — Initial	$J_f - J_i$
44	4255.6	4255.28	101	$3d'\ ^2G - 4f^1\ ^2H^o$	7/2 - 9/2
57	4380.7	4379.96	102	$3d'\ ^2D - 4f^1\ ^2F^o$	5/2 - 7/2
57	4380.7	4379.56	102	$3d'\ ^2D - 4f^1\ ^2F^o$	3/2 - 5/2
57	4380.7	4379.96	102	$3d'\ ^2D - 4f^1\ ^2F^o$	5/2 - 5/2
40	4144.1	4143-4147	106	$3p\ ^6P - 3d\ ^6D^o$	band
71	4467.2	4467.64	87	$3d\ ^2P - 4f\ ^4D^o$	3/2 - 3/2
74	4476.3	4477.28	87	$3d\ ^2P - 4f\ ^4D^o$	1/2 - 3/2
71	4467.2	4466.72	94	$3s\ ^6S^o - 3p\ ^6P$	5/2 - 7/2
72	4469.1	4469.20	94	$3s\ ^6S^o - 3p\ ^6P$	5/2 - 5/2
73	4470.3	4470.65	94	$3s\ ^6S^o - 3p\ ^6P$	5/2 - 3/2

Table 2. Wavelengths and Transitions of Lines Observed in Ionization State O III.

Line No.	Measured Wavelength (Å)	Identified Wavelength (Å)	Multiplet	Transition Final	Initial	$J_f - J_i$
15	3760.8	3760.95	2	$3s\ ^3P^o$	$3p\ ^3D$	2 - 3
13	3755.8	3755.73	2	$3s\ ^3P^o$	$3p\ ^3D$	1 - 2
14	3758.4	3758.27	2	$3s\ ^3P^o$	$3p\ ^3D$	0 - 1
17	3792.4	3792.33	2	$3s\ ^3P^o$	$3p\ ^3D$	2 - 2
16	3774.8	3775.07	2	$3s\ ^3P^o$	$3p\ ^3D$	1 - 1
18	3811.7	3812.04	2	$3s\ ^3P^o$	$3p\ ^3D$	2 - 1
3	3704.2	3704.40	21	$3s\ ^5P$	$3p\ ^5D^o$	3 - 4
2	3699.5	3699.75	21	$3s\ ^5P$	$3p\ ^5D^o$	2 - 3
1	3696.6	3696.41	21	$3s\ ^5P$	$3p\ ^5D^o$	1 - 2
6	3721.7	3721.95	21	$3s\ ^5P$	$3p\ ^5D^o$	3 - 3
5	3713.3	3713.50	21	$3s\ ^5P$	$3p\ ^5D^o$	2 - 2
7	3721.5	3722.97	21	$3s\ ^5P$	$3p\ ^5D^o$	2 - 1
4	3709.1	3710.59	21	$3s\ ^5P$	$3p\ ^5D^o$	1 - 0
70	4463.1	4462.76	33	$3p\ ^5S^o$	$3d\ ^5P$	2 - 3
68	4449.2	4449.06	33	$3p\ ^5S^o$	$3d\ ^5P$	2 - 2
67	4435.6	4435.60	33	$3p\ ^5S^o$	$3d\ ^5P$	2 - 1
74	4476.3	4476.30	37	$3p\ ^1D^o$	$3d\ ^1D$	2 - 2

Table 3. Wavelengths and Transitions of Lines Observed in Ionization State O IV.

Line No.	Measured Wavelength (Å)	Identified Wavelength (Å)	Multiplet	Transition Final	Initial	$J_f - J_i$
11	3737.6	3737.84	6	$3p\ ^4D$	$3d\ ^4F^o$	7/2 - 9/2
10	3729.9	3730.09	6	$3p\ ^4D$	$3d\ ^4F^o$	5/2 - 7/2
8	3726.6	3726.88	6	$3p\ ^4D$	$3d\ ^4F^o$	3/2 - 5/2
8	3726.6	3726.88	6	$3p\ ^4D$	$3d\ ^4F^o$	1/2 - 3/2

Table 4. Normalized Relative Powers as a Function of Particle Energy

Line Number	Transition Final — Initial	P' at Particle Energy (MeV) 0.20	0.40	0.50	0.63	0.75	0.87	1.00
	O II							
51	$3s\ ^4P_{5/2} - 3p\ ^4P^o_{5/2}$			12.0				
54	$3s\ ^4P_{5/2} - 3p\ ^4P^o_{3/2}$			8.3				
50	$3s\ ^4P_{3/2} - 3p\ ^4P^o_{1/2}$			11.3		5.8		
12	$3s\ ^4P_{5/2} - 3p\ ^4S^o_{3/2}$	2.4	3.9	5.9	4.3			
9	$3s\ ^4P_{3/2} - 3p\ ^4S^o_{3/2}$	1.9	3.5					
29	$3s\ ^2P_{3/2} - 3p\ ^2P^o_{3/2}$	4.3	6.2	8.0	6.9	4.8		
27	$3s\ ^2P_{1/2} - 3p\ ^2P^o_{1/2}$	2.3	3.2	5.0	6.3			
34	$3p\ ^4D^o_{7/2} - 3d\ ^4F_{9/2}$	6.1	8.2	13.4		6.5	6.9	5.6
36	$3p\ ^4D^o_{5/2} - 3d\ ^4F_{5/2}$		3.0	4.7				
39	$3p\ ^4P^o_{5/2} - 3d\ ^4D_{7/2}$	4.1	5.8	8.1	6.9	6.6		
43	$3p'^2F^o_{7/2} - 3d'^2G_{9/2}$	4.6	9.4	12.5	11.7	8.0		
42	$3p'^2F^o_{5/2} - 3d'^2G_{7/2}$	4.3	5.2	11.2	10.7	6.0		
49	$3d\ ^2F_{7/2} - 4f\ ^2G^o_{9/2}$			7.6	8.2			

Table 4---Continued

Line Number	Transition Final	Initial	P' at Particle Energy (MeV) 0.20	0.40	0.50	0.63	0.75	0.87	1.00
	O III								
15	$3s\ ^3P^o_2$	$3p\ ^3D_3$	4.3	12.2	18.0	19.9	17.3	12.9	10.1
13	$3s\ ^3P^o_1$	$3p\ ^3D_2$	2.8	8.4	13.8	12.6	13.4	7.8	6.3
17	$3s\ ^3P^o_2$	$3p\ ^3D_2$	0.9	3.6	5.2	4.6	4.3		
16	$3s\ ^3P^o_1$	$3p\ ^3D_1$	1.0	3.9	6.4	7.9	6.2	4.6	3.3
3	$3s\ ^5P_3$	$3p\ ^5D^o_4$	2.4	7.8	12.9	12.7	13.4	9.0	7.8
2	$3s\ ^5P_2$	$3p\ ^5D^o_3$	1.1	4.4	8.8	6.6	7.8	4.8	3.3
1	$3s\ ^5P_1$	$3p\ ^5D^o_2$			5.3	4.0	2.7		1.9
6	$3s\ ^5P_3$	$3p\ ^5D^o_3$	1.2	2.9	5.6	4.9	4.6	3.5	2.0
5	$3s\ ^5P_2$	$3p\ ^5D^o_2$	1.4	3.5	6.7	5.5	6.5	4.3	3.0
	O IV								
11	$3p\ ^4D_{7/2}$	$3d\ ^4F^o_{9/2}$			6.9	6.3	9.6	7.6	7.7
10	$3p\ ^4D_{5/2}$	$3d\ ^4F^o_{7/2}$				7.0	8.6	6.2	6.3

Table 5. Relative Populations of Levels as a Function of Energy.

Line No.	Initial Level	N' at Particle Energy (MeV)						
		0.20	0.40	0.50	0.63	0.75	0.87	1.00
	O II							
51	$3p\ {}^4P^o_{5/2}$			7.3				
54	$3p\ {}^4P^o_{3/2}$			7.3				
50	$3p\ {}^4P^o_{1/2}$			5.6	2.8			
12	$3p\ {}^4S^o_{3/2}$	2.5	4.0	6.1	4.5			
9	$3p\ {}^4S^o_{3/2}$	1.3	2.4					
29	$3p\ {}^2P^o_{3/2}$	1.4	2.0	2.6	2.2	1.6		
27	$3p\ {}^2P^o_{1/2}$	0.9	1.3	2.0	1.4			
34	$3d\ {}^4F_{9/2}$	0.8	1.1	1.8		0.9	0.9	0.7
36	$3d\ {}^4F_{5/2}$		2.5	4.0				
39	$3d\ {}^4D_{7/2}$	0.6	0.9	1.2	1.0	1.0		
43	$3d'\ {}^2G_{9/2}$	0.6	1.3	1.7	1.6	1.1		
42	$3d'\ {}^2G_{7/2}$	0.6	0.7	1.4	1.4	0.8		
49	$4f\ {}^2G^o_{9/2}$			0.9	0.9			

Table 5.---Continued.

Line No.	Initial Level	N' at Particle Energy (MeV)						
		0.20	0.40	0.50	0.63	0.75	0.87	1.00
	O III							
15	$3p\ ^3D_3$	0.8	2.2	3.2	3.6	3.1	2.3	1.8
13	$3p\ ^3D_2$	0.5	1.4	2.3	2.1	2.2	1.3	1.0
17	$3p\ ^3D_2$	1.3	5.2	7.6	6.6	6.3		
16	$3p\ ^3D_1$	0.9	3.4	5.5	6.8	5.4	4.0	2.9
3	$3p\ ^5D^o_4$	0.5	1.6	2.6	2.6	2.7	1.8	1.6
2	$3p\ ^5D^o_3$	0.3	1.1	2.2	1.7	2.0	1.2	0.8
1	$3p\ ^5D^o_2$			1.8	1.4	0.9		0.6
6	$3p\ ^5D^o_3$	1.2	3.0	5.6	4.9	4.7	3.5	2.0
5	$3p\ ^5D^o_2$	0.8	2.0	3.8	3.1	3.7	2.5	1.7
	O IV							
11	$3d\ ^4F^o_{9/2}$			2.0	1.8	2.8	2.2	2.3
10	$3d\ ^4F^o_{7/2}$				2.1	2.5	1.8	1.9

Table 6. "Non-degenerate State Populations" of Transitions Observed With 0.50 MeV Particles.

Line No.	Level	Energy above Ground Level of O II (cm^{-1})	$\frac{N' \times 10}{(2S+1)(2J+1)}$
	O II		
50	$3p\ {}^4P^o_{1/2}$	208,346	6.9
54	$3p\ {}^4P^o_{3/2}$	208,393	4.6
51	$3p\ {}^4P^o_{5/2}$	208,484	3.0
12	$3p\ {}^4S^o_{3/2}$	212,162	3.8
27	$3p\ {}^2P^o_{1/2}$	214,169	5.0
29	$3p\ {}^2P^o_{3/2}$	214,229	3.3
36	$3d\ {}^4F_{5/2}$	231,350	1.7
34	$3d\ {}^4F_{9/2}$	231,350	0.44
39	$3d\ {}^4D_{7/2}$	232,754	0.35
43	$3d'\ {}^2G_{9/2}$	252,608	0.87
42	$3d'\ {}^2G_{7/2}$	252,609	0.87
49	$4f\ {}^2G^o_{9/2}$	255,984	0.43
	O III		
13	$3p\ {}^3D_2$	577,552	1.5
15	$3p\ {}^3D_3$	577,772	1.5
1	$3p\ {}^5D^o_2$	649,170	0.72
2	$3p\ {}^5D^o_3$	649,270	0.63
3	$3p\ {}^5D^o_4$	649,347	0.58
	O IV		
11	$3d\ {}^4F^o_{9/2}$	1,221,997	0.50

Table 7. Comparison of Ratios of Line Strengths to Ratios of Powers for Selected Lines.

Line No.	Transition Final	Initial	Line Strength (relative)	Ratio of Line Strengths	Average Ratio of Powers
1	$3s\ ^5P_1$	$- 3p\ ^5D^o_2$	19.4	0.60	0.67
5	$3s\ ^5P_2$	$- 3p\ ^5D^o_2$	32.4		
2	$3s\ ^5P_2$	$- 3p\ ^5D^o_3$	51.9	2.00	1.50
6	$3s\ ^5P_3$	$- 3p\ ^5D^o_3$			
13	$3s\ ^3P^o_1$	$- 3p\ ^3D_2$	53.6	3.00	2.75
17	$3s\ ^3P^o_2$	$- 3p\ ^3D_2$			
9	$3s\ ^4P_{3/2}$	$- 3p\ ^4S^o_{3/2}$	20.0	0.67	0.84
12	$3s\ ^4P_{5/2}$	$- 3p\ ^4S^o_{3/2}$	30.0		

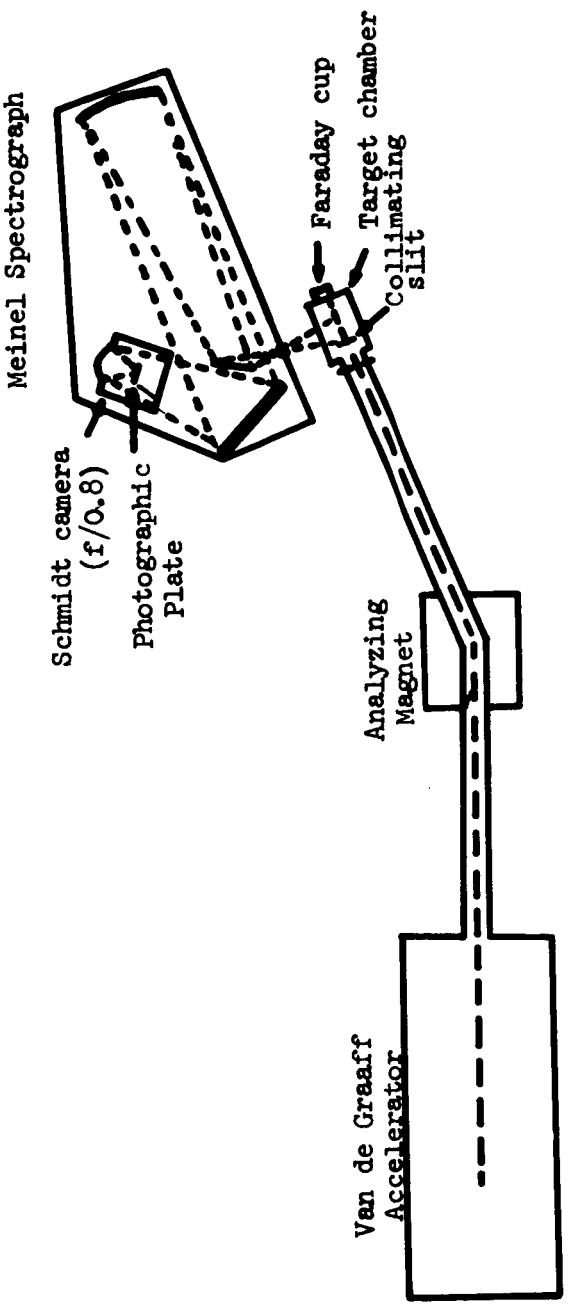

Figure 1. Schematic for the experiment.

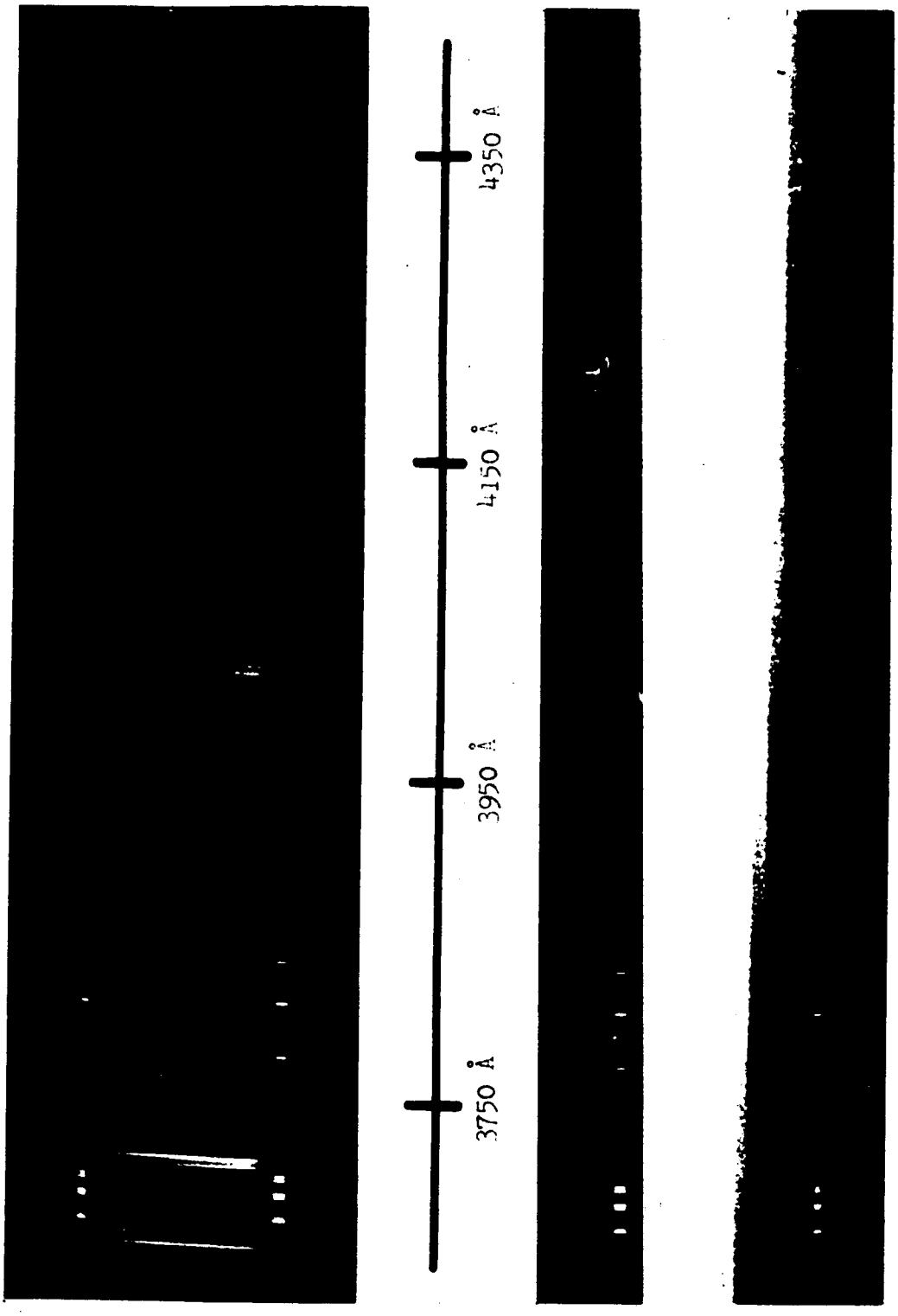

Figure 2. Spectral plate taken with 1.0 MeV beam and corresponding black-body plate.

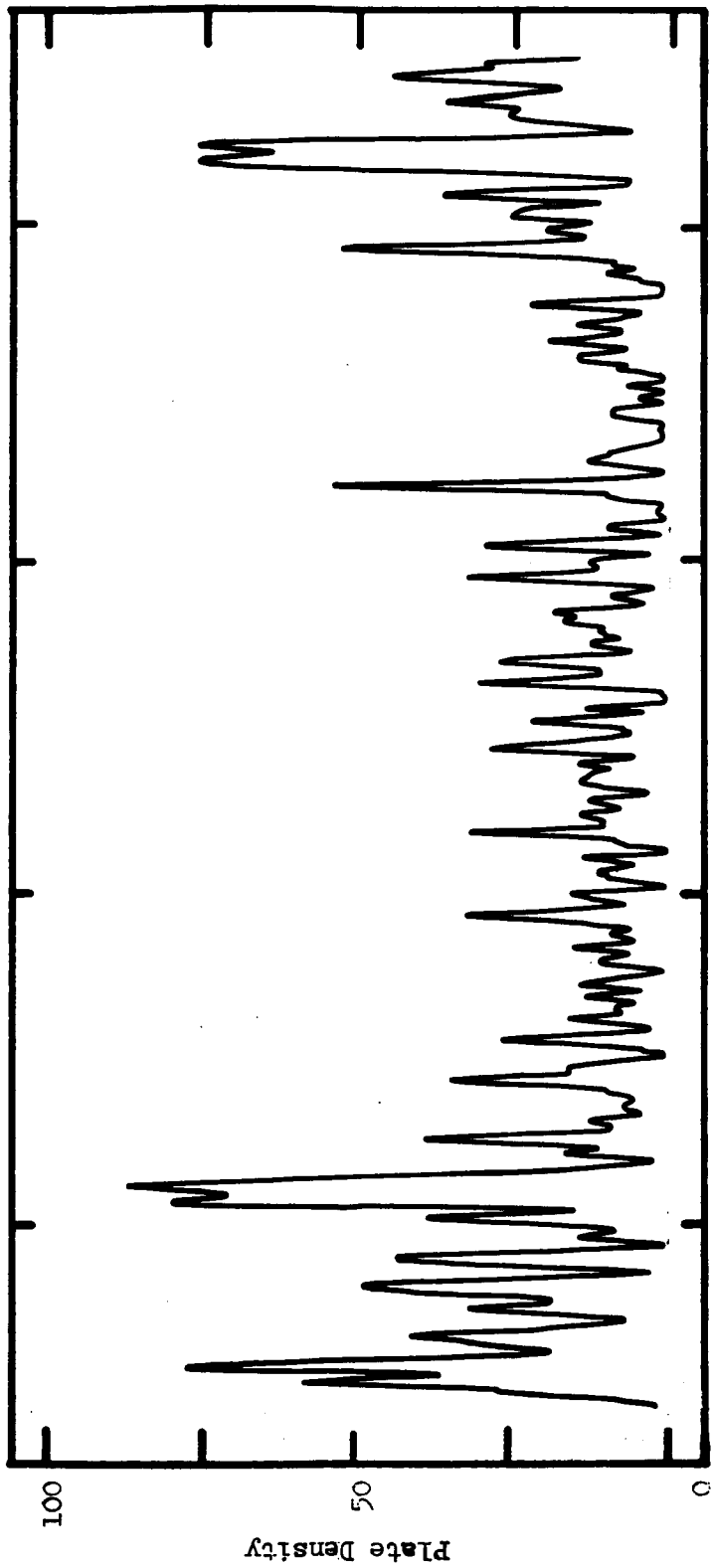

Figure 3. Densitometer scan of a spectral plate.

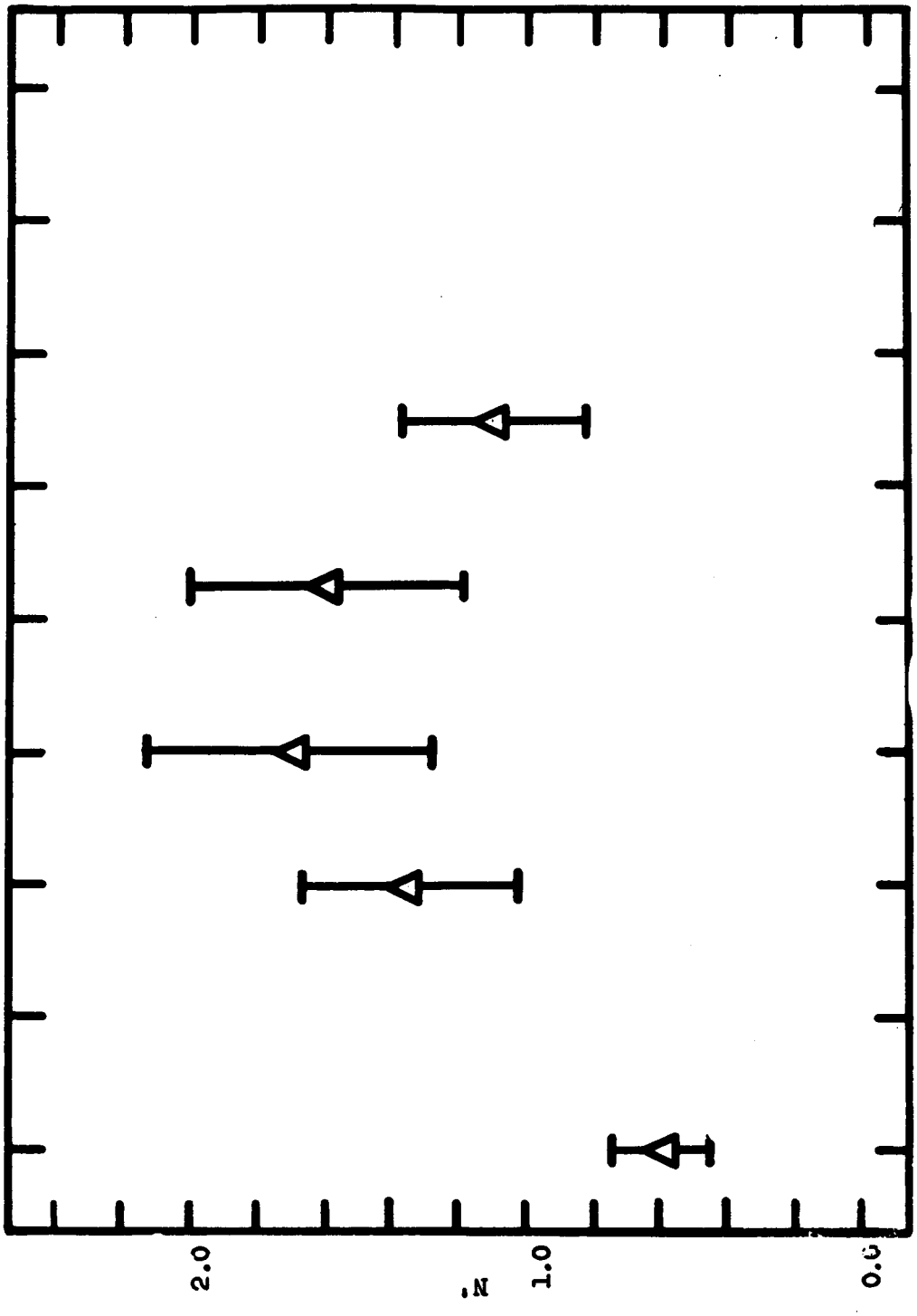

Figure 4. Excitation function for O II, level $3d'\ ^4G_{9/2}$.

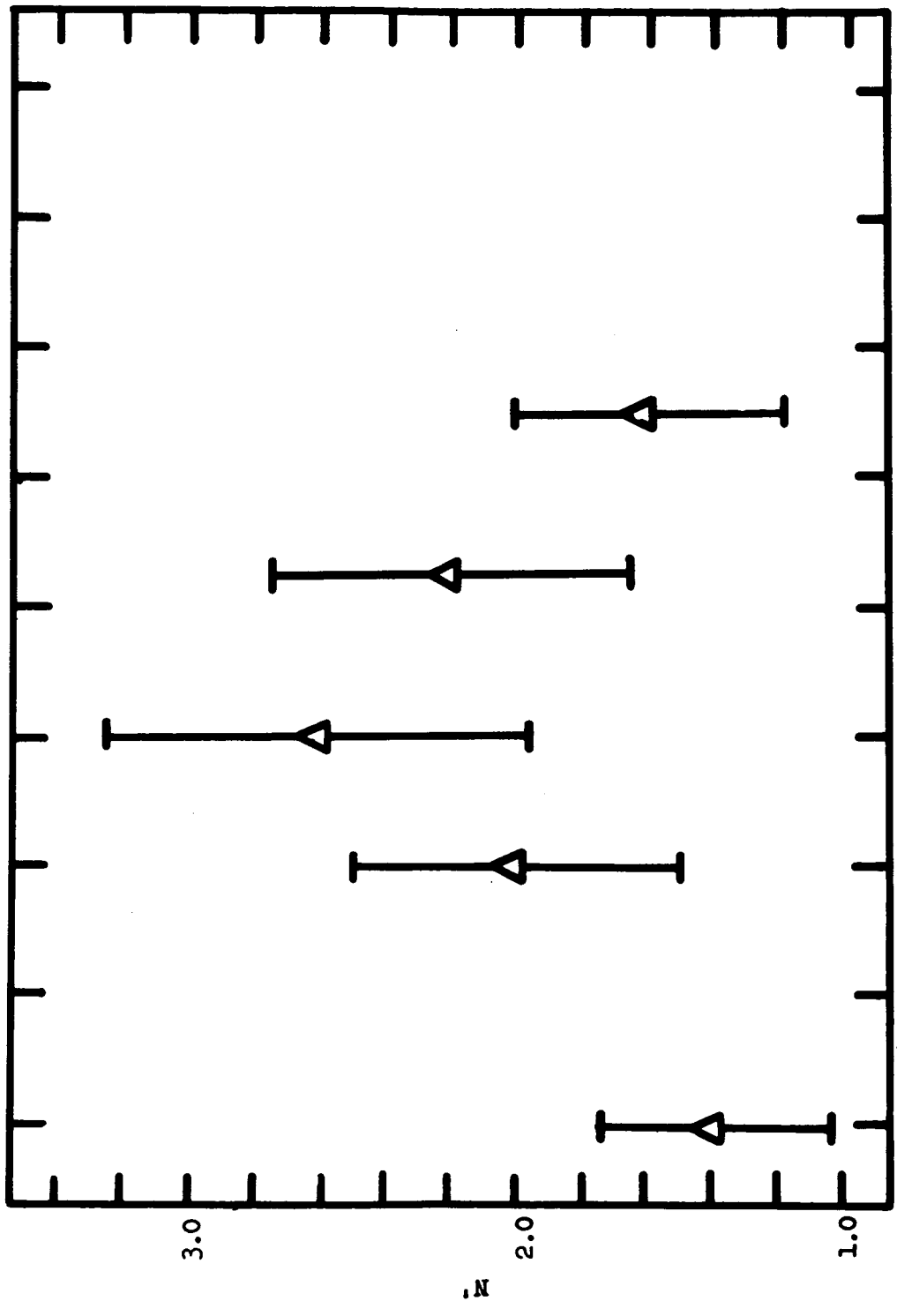

Figure 5. Excitation function for O II, level 3p $^3P^o_{3/2}$.

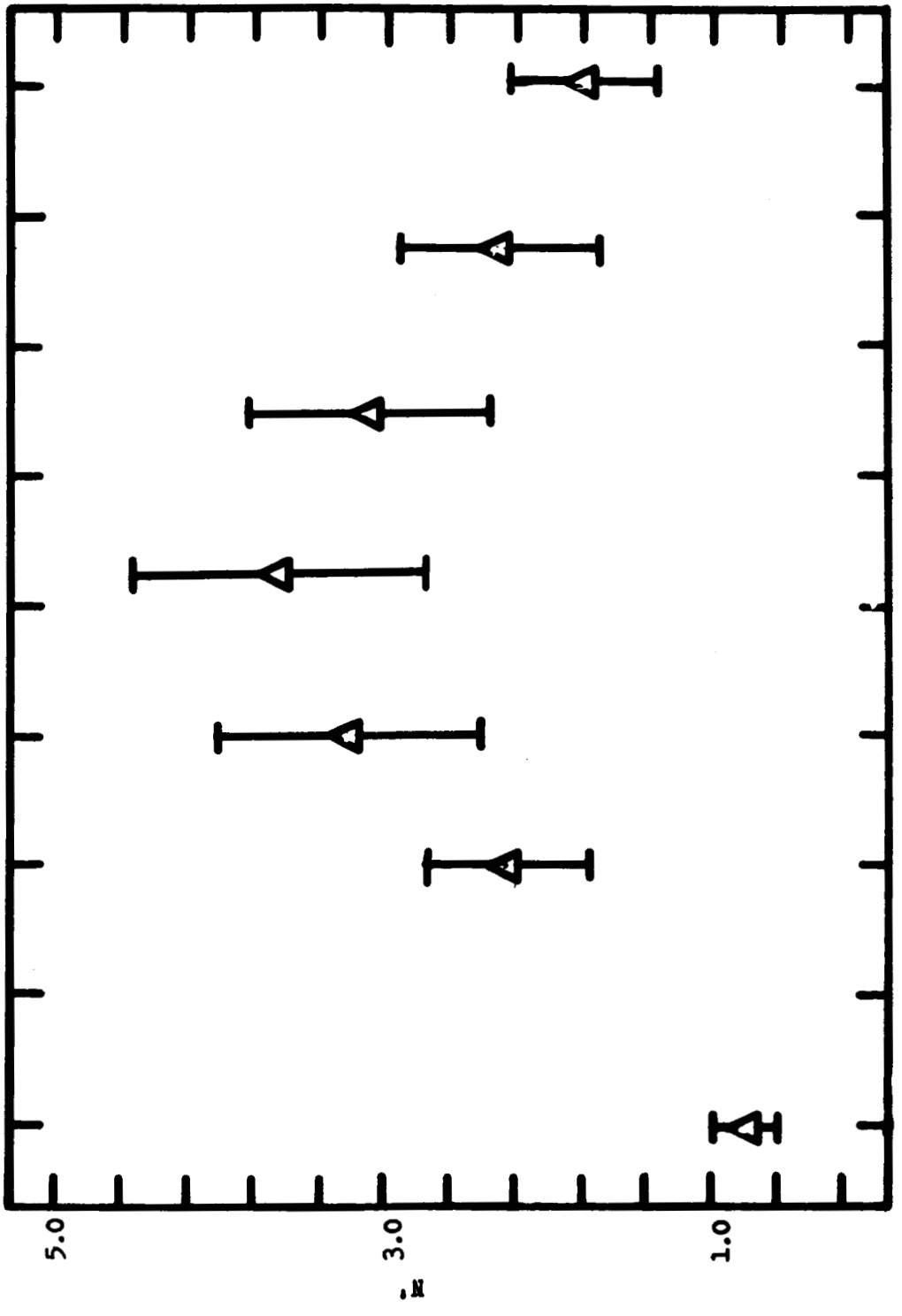

Figure 6. Excitation function for O III, level 3p $^3D_3$.

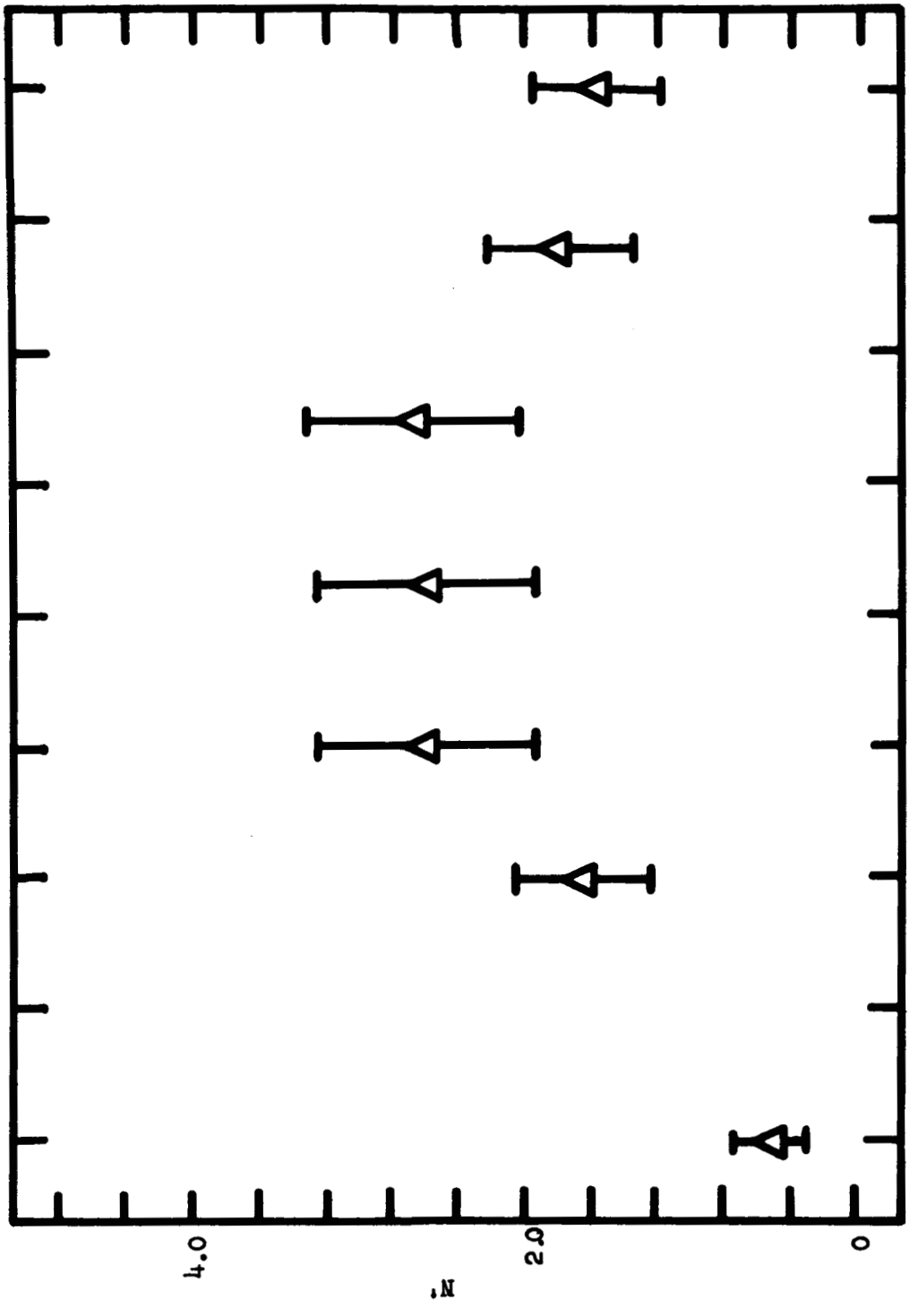

Figure 7. Excitation function for O III, level 3p $^5D_4^o$.

LIST OF REFERENCES

[1]Bashkin, S., and Meinel, A., Astrophysical Journal 139, 413 (1964).

[2]Harrison, G. R., Lord, R. C., and Loofbourow, J. R., Practical Spectroscopy, (Prentics-Hall, Inc. 1948).

[3]Smith, W. S., Unpublished communication, 1967.

[4]Moore, Charlotte E., A Multiplet Table of Astrophysical Interest, U. S. Department of Commerce, 1945.

[5]Moore, Charlotte E., Atomic Energy Levels, Vol. 1, U. S. Department of Commerce, 1949.

[6]Wiese, W. L., Smith, M. W., and Glennon, B. M., Atomic Transition Probabilities, Vol. I, National Bureau of Standards, 1966.

[7]Condon, E. U., and Shortley, G. H., The Theory of Atomic Spectra, (Cambridge University Press, 1951).